In situ visualization of aortic dissection propagation in notched rabbit aorta using synchrotron X-ray tomography

J. Brunet, Baptiste Pierrat, J. Adrien, E. Maire, B.A. Lane, N. Curt, A. Bravin, N. Laroche, P. Badel

In situ visualization of aortic dissection propagation in notched rabbit aorta using synchrotron X-ray tomography

J. Brunet[1,*], B. Pierrat[1,*], J. Adrien[2], E. Maire[2], B. A. Lane[1], N. Curt[1], A. Bravin[3], N. Laroche[4], and P. Badel[1]

[1]Mines Saint-Etienne, Univ Lyon, Univ Jean Monnet, INSERM, U 1059 Sainbiose, Centre CIS, F - 42023 Saint-Etienne France

[2]Université de Lyon, INSA-Lyon, MATEIS CNRS UMR5510, Villeurbanne, France

[3]European Synchrotron Radiation Facility (ESRF), Grenoble, France

[4]University of Lyon, Jean Monnet University, INSERM, U1059 Sainbiose, 42023, Saint-Etienne, France

[*]Corresponding authors: Baptiste Pierrat (pierrat@emse.fr), Joseph Brunet (jo.brunet73@gmail.com)

Abstract

Aortic dissection is a complex, intramural, and dynamic condition involving multiple mechanisms, hence, difficult to observe. In the present study, a controlled in vitro aortic dissection was performed using tension-inflation tests on notched rabbit aortic segments. The mechanical test was combined with conventional (cCT) and synchrotron (sCT) computed tomography for in situ imaging of the macro- and micro-structural morphological changes of the aortic wall during dissection. We demonstrate that the morphology of the notch and the aorta can be quantified in situ at different steps of the aortic dissection, and that the notch geometry correlates with the critical pressure. The phenomena prior to propagation of the notch are also described, for instance the presence of a bulge at the tip of the notch is identified, deforming the remaining wall. Finally, our method allows us to visualize for the first time the propagation of an aortic dissection in real-time with a resolution that has never previously been reached.

Keywords: Aortic dissection; synchrotron X-ray tomography; tear propagation; tension-inflation test; in situ testing

1 Introduction

Aortic dissection is the most common catastrophic event affecting the aorta, with an incidence of 35 cases per 100,000 people per year in people aged 65-75 years [1]. This condition is characterized by a tear in the innermost layer of the aortic wall, allowing blood to flow between the layers of the aorta and creating a false lumen. The dissection can propagate either in the antegrade or retrograde direction from a pre-existing defect in the medial section of the arterial wall. Most of the time, the resulting intimal tear forms in the circumferential direction ($> 80\%$) [2] and propagates in the outer third media [3]. The pathogenesis of aortic dissection is believed to involve medial degeneration combined with mechanical fatigue [4]. Elastic fiber degeneration leading to loss of fiber integrity [5–7], as well as loss of functional smooth muscle cells [8,9] were observed in patients and animal models with a dissected aorta. However, these observations were the result of post-mortem analysis and the exact causes leading to the formation of a tear and its propagation are not completely identified.

In contrast, the propagation of a tear is a purely dynamic process that can be modeled experimentally by reproducing the dissection event in a controlled manner. As a result, several mechanical tests were used to quantify the dissection properties of the aorta, including radial testing [10], peeling testing [10, 11], shear testing [12], and liquid infusion testing [13, 14]. However, these mechanical tests are considerably different from in vivo conditions thus preventing definitive conclusions for an accurate mechanical description of the dissection. Furthermore, no satisfactory in situ visualization of an in vivo or in vitro aortic dissection was performed during the failure event. Only images of already dissected aortas can be found in literature. As a consequence, the morphological changes of the macro- and micro-structure of the aortic wall during the initiation and propagation of a dissection remain poorly understood. It should be emphasized that microstructure (e.g. lamellae architecture) plays a crucial role during aortic dissection. A method observing the in situ initiation and propagation of an aortic dissection in order to quantify geometrical changes and fracture modes is required.

The main challenges preventing in situ observation of this condition are that the failure process is intramural, acute [4, 15], and difficult to reproduce experimentally. Although there has been tremendous progress made in the imaging techniques of biological tissues, most of them remain limited by either resolution or field of view for the visualization of aortic dissection [16]. For instance, confocal microscopy and optical coherence tomography could assess the 3D strain field of the aortic microstructure; however, these imaging approaches can only be applied to a very restricted depth due to the opacity of the tissue, preventing a global observation of the aorta [17–19]. The same limitation concerning the field of view applies to electron microscopy [17] and multiphoton microscopy [20, 21]. On the other hand, magnetic resonance imaging provides a sufficient field

of view to visualize the entire aorta but is limited in terms of spatial and temporal resolution [22]. High-resolution ultrasound imaging is also restricted by its spatial resolution, which prevents the direct observation of the microstructural components in the aortic wall. [22].

X-ray computed tomography is a non-destructive approach, allowing observations of the aortic microstructure with high resolution and a field of view larger than the aortic diameter. This imaging technique has previously been used to visualize in situ uniaxial tension tests [23] and tension-inflation tests [24] with a voxel size between 4 and 7 µm. In addition, synchrotron X-ray computed tomography can achieve an even higher spatial and temporal resolution for an equivalent field of view, allowing the global structure and microstructure of the aorta to be observed simultaneously. This was demonstrated by Trachet et al. [25], where the authors inflated mice aortas and used in situ sCT to quantify the morphology of the medial lamellae at different pressures. However, this study remained at physiological pressure and did not investigate failure. Logghe et al. [26] observed aortic dissection evolution using sCT in genetically-modified mouse models at multiple stages of the disease, but this method does not enable the observation of the dissection propagation.

In the present study, a tension-inflation test was performed on notched rabbit aortas in order to create an in vitro dissection. During this mechanical test, the 3D microstructure of the aortic specimens was visualized in situ using conventional and synchrotron X-ray tomography. The objective was to observe and quantify the evolution of the aortic and notch morphology during the dissection process in order to provide a better understanding of the phenomena behind the initiation and propagation of aortic dissection.

2 Materials and methods

2.1 Sample preparation

Female 11 19-week-old New Zealand white rabbits were sacrificed by carbon dioxide inhalation following the EU Directive 2010/63/EU for animal experiments. The descending aorta from the left subclavian artery to the diaphragm was carefully excised just after death. Rabbits were chosen over mice or rats due to their better resemblance to humans in terms of aortic microstructure [27, 28]. In addition, the size of the rabbit aorta provides a very good trade-off between resolution and field of view with X-ray microtomography. The typical length of the samples was 50 mm. The branches were sutured with silk wire with the help of a dissecting scope. During this process, the aortas were immersed in phosphate-buffered saline (PBS) to avoid tissue dehydration. The samples were subsequently frozen at -20°C for future use. The 6 samples observed with cCT were immersed for 12 hours in a diluted solution of sodium polytungstate (15 g/L) at 4 °C to ensure a good contrast on the X-ray tomography images [23]. No contrast agent was used for sCT.

The day of the test, after defrosting at room temperature, the aorta was turned inside out and a notch was created on the intimal side of the specimen, on the opposite side of the intercostal branches, with a micro dissecting knife, in order to model a pre-existing defect within the intimal and medial layers. The term "notch" will then specifically refer to this artificial initial defect, in contrast to the term "tear", referring to the entry site post-dissection. The notches were made by the same operator for better consistency. They were cut in two orientations: circumferential ($n = 9$) and longitudinal ($n = 2$). Each end of the sample was then attached to hydraulic connectors using silk wire and mounted on the tension-inflation device.

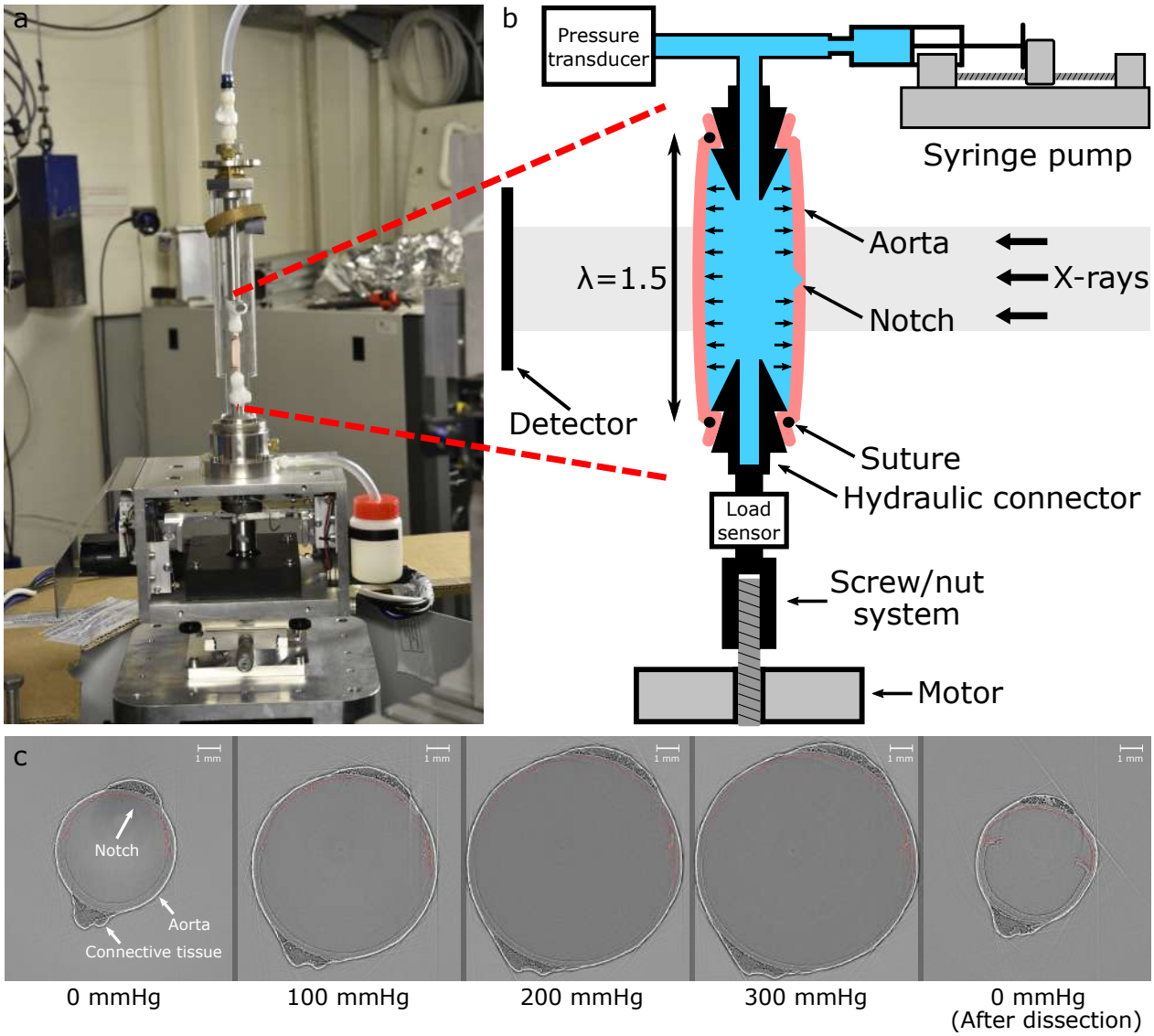

Figure 1: **In situ tension-inflation test on notched rabbit aorta**. (**a**), Experimental set-up on the beamline sample stage at the biomedical beamline ID17 of the European Synchrotron Radiation Facility (ESRF). (**b**), Schematic of the in situ tension-inflation setup with the notched rabbit aorta and all the main components of the custom-made device, including the syringe pump to inflate the sample and the screw-nut system to apply the axial pre-stretch. λ is the stretch applied to the aorta. (**c**), High-resolution sCT cross-sections of a rabbit aortic specimen at 0, 100, 200, 300 mmHg and after dissection with an isotropic voxel size of 3.02 µm. The circumferential notch is highlighted in red. The sCT images obtained during the aorta inflation at different pressure steps and after dissection are presented in Supplementary Video 1.

2.2 Custom-made tension-inflation device

Our custom-made in situ tension-inflation rig (Figure 1a,b) was designed to be compatible with both cCT and sCT setups. The specimen was enclosed in a 50 mm diameter cylindrical PMMA tube, which only slighlty absorbs X-rays. Sample dehydration was prevented by saturating the tube chamber with mist using

a humidifier prior to the mechanical test. A rotating motor coupled with a screw/nut system ensured the stretch of the specimen with a maximum displacement of 50 mm and a maximum displacement rate of 1.25 mm/s. A syringe pump infused PBS into the aorta to increase the pressure at a quasi-static flow rate of 5 ml/min. A load sensor (LCM201, Omega™, 300 N) and a pressure sensor (PXM319, Omega™, 0 - 3.5 bar) recorded the pressure and the axial load during the mechanical test. Custom-made software was created to control the device. A proportional–integral–derivative controller (PID controller) was integrated into the control software in order to maintain a constant pressure during the X-ray scan, thus minimizing viscoelastic effects or compensating possible leaks.

2.3 Conventional X-ray micro-tomography

N=4 samples with a circumferential notch and n=2 samples with a longitudinal notch were visualized with cCT. We used a Phoenix^{TM} VtomeX tomograph, described in Buffiere et al. [29], equipped with a Varian^{TM} Paxscan X-Ray detector of size 1920 x 1536 pixels. The X-ray tomography setup was powered at a voltage of 80 kV and a current of 370 µA. The total acquisition time was 180 seconds and the number of projections was 900. The voxel size was 7 x 7 x 7 µm^3 and the field of view was 10.5 x 10.5 x 8.75 mm^3. The reconstruction was performed using a filtered back-projection algorithm.

2.4 Synchrotron X-ray micro-tomography

N=5 samples with a circumferential notch were visualized with sCT. The experiments were performed at the biomedical beamline ID17 of the European Synchrotron Radiation Facility (ESRF) in Grenoble, France. Ultra-high-resolution imaging was achieved by using phase-contrast X-ray imaging with a quasi-parallel laminar monochromatic 40-keV X-ray beam and a single propagation distance of 2 m. No contrast agent was used. The imaging detector was a PCO.edge 5.5 sCMOS camera (Kelheim, Germany) coupled to a 250 µm thick LuAG:Ce scintillator. The number of projections and the acquisition time for a scan were 4000 and 240 seconds, respectively. The field of view was increased by performing the scans in half-acquisition mode, with the center of rotation on the left side of the projections. The voxel size and the field of view were 3.02 x 3.02 x 3.02 µm^3 and 15.3 x 15.3 x 6.5 mm^3, respectively. The scan of the sample in the dissected state was performed in three steps to increase the axial field of view to 15.3 x 15.3 x 15 mm^3. The reconstruction was performed using a filtered back-projection algorithm, coupled with single-distance phase retrieval [30] and a 2D unsharp mask.

2.5 Protocol

Once the sample was attached to the device, two radiographic images of the sample in the unloaded configuration were taken at 0 and 90 degrees to measure the initial diameter of the sample. Then, an axial pre-stretch of 1.5 was applied to the specimen to reproduce the physiological state. This value was quantified with previous experiments so that the axial load at physiological pressure was null. The axial pre-stretch was kept constant throughout the rest of the experiment. Subsequently, 3D scans were taken at a pressure of 0, 100, 200, and 300 mmHg. The pressure was held for 5 min before the scan in order to compensate creep effects. Then, the pressure was increased until dissection while observing the specimen with radiographic images at a frame rate of 5 images per second for conventional imaging and 50 images per second for synchrotron imaging. A final scan was performed after dissection of the sample at 0 mmHg.

2.6 Histology

After the in situ tension-inflation test, aortic specimens were fixed in Ethanol 80% at 4°C and routinely processed for paraffin embedding and cross-sectioned to obtain 5 µm-thick sections (Microtome Leica RM2245, Feather Microtome blade N35HR). Before use, sections were deparaffinized, rehydrated and processed for histochemical staining. The slides were incubated with a 1% Sirius Red solution dissolved in aqueous saturated picric acid for 30 minutes, washed in acidified water (0.5% hydrogen chloride), dehydrated and mounted with Entellan® medium. Collagen type I and III were red stained.

2.7 Data processing

The morphology of the notch was quantified with three metrics: the notch depth, the notch width (measured by the angle of the notch in the circumferential direction), and the dissection length (measured in the longitudinal direction). The notch depth was normalized with the medial thickness to allow a comparison between specimens and to take into account the decrease in aortic thickness during inflation: the value ranges between 0 (intimal side) and 100 (adventitial side). The different measurements were taken manually with the software imageJ [31, 32]. The mean of at least three measures was taken as the final value to avoid local effects. Diameter measurements were taken far from the notch for the same reason. The segmentation of the aorta and the 3D representation were performed using 3D Slicer [33]. ParaView software [34] was used for 3D display.

2.8 Stretch-stress calculations

The circumferential stretch of the aortic wall λ_θ was calculated by

$$\lambda_\theta = \frac{r_m}{r_m^0}\,, \tag{1}$$

where r_m is the current midwall radius of the aorta and r_m^0 is the initial midwall radius at 0 mmHg of pressure. The aortic wall was assumed thin (diameter/thickness > 20). As a consequence, the circumferential Cauchy stress σ_θ was calculated by

$$\sigma_\theta = \frac{r_m\, P}{h}\,, \tag{2}$$

where P is the internal pressure and h is the current wall thickness. Note that this represents a wall-averaged stress as no distinction was made between the different layers of the artery. A paired Student's t-test was performed to assess the difference between the aortic thickness before and after propagation of the dissection.

2.9 Statistical Analysis

A Student's t-test was performed to assess the linear correlation between the critical pressure and the notch depth, the notch width, and the dissection length. A paired t-test was used to evaluate the significance of the difference between the thickness of the aortic wall before and after dissection.

3 Results

3.1 cCT and sCT imaging of inflated notched rabbit aortic segments

The tension-inflation test was performed using our custom-made device (Figure 1a) inside the cCT and sCT setups. The cCT combined with the contrast agent provides images with sufficient contrast to distinguish the media, adventitia and connective tissue. A contrast agent was not required for sCT as the spatial coherence of the beam provides sufficient propagation-based phase contrast to visualize the medial lamellae and intima in addition to the media, adventitia and connective tissue. The acquisition time was kept as low as possible (180 to 240 seconds) to avoid possible sample motion. The field of view was sufficient to observe the entire circumference of the aorta, even at high pressure. By satisfying the trade-off between spatial resolution, field of view, and acquisition time, our methodology enabled the observation of the complete aortic dissection sequence with an unprecedented resolution (Figure 1c and Supplementary Video 1). Images acquired by cCT are presented in Supplementary Figures S1 and S2.

3.2 Critical pressure and dissection analysis

The notch propagated in all the aortic specimens (n=11) for critical pressures ranging from 226 to 902 mmHg. Conventional computed tomography was used to visualize n=4 circumferentially-notched samples and n=2 longitudinally-notched samples, whereas n=5 circumferentially-notched samples were observed with sCT. Local propagation of the crack was visualized at different stages of the inflation; however, the critical pressure was taken as the pressure at which the notch propagates throughout the segment. The mean critical pressure was 595 ± 189 mmHg (Mean ± SD, n = 9) and 685 ± 88 mmHg (n = 2) for the notch in the circumferential and longitudinal direction, respectively. Three samples dissected before 300 mmHg. In most specimens, the external wall of the false lumen ruptured after dissection, resulting in vessel failure. The same phenomenon is observed clinically as the rupture mostly appears in the false channel due to the small thickness of the outer wall [2, 35]. Interestingly, samples dissected before 300 mmHg did not exhibit rupture of the false lumen and were able to maintain 300 mmHg pressure and above, as shown in Figure 6.

Figure 2 shows a 3D view with three cross-sections of a representative dissected specimen. The flap resulting from the dissection of the sample is clearly visible. It should be noted that the sCT images, such as cross-sections in Figure 2b, are similar to those that may be observed clinically, thus validating our methodology for visualizing aortic dissection. The exact dissection length could not be assessed due to the limited field of view of the cCT and sCT in the longitudinal direction. In the distal direction, the notches propagated outside the field of view for all samples. However, from visual observation, the dissection extended from the notch to the distal part of the descending aorta sutured to the hydraulic connector. In the proximal direction, the dissection extended out of the field of view for n=5 samples and only over a few millimeters for n=6 specimens. No re-entry tear was identified.

A comparison of sCT and histology images of a dissected descending aorta is presented in Figure 3. The lamellae observed with sCT correspond to the structure observed in histological images, demonstrating that sCT can be used as a virtual histology tool to study aortic dissection. In the present study, the dissection almost always involved half to three quarters of the aortic circumference. During dissection, delamination occured between medial lamellae, however they rarely fractured. The sCT images revealed, and the histology confirmed, that the dissection spreads over approximately three to four medial lamellae, corresponding to 16-21% of the thickness of the aortic wall (Figure 3). An example of a specimen with a longitudinal notch is presented in Supplementary Figure S2.

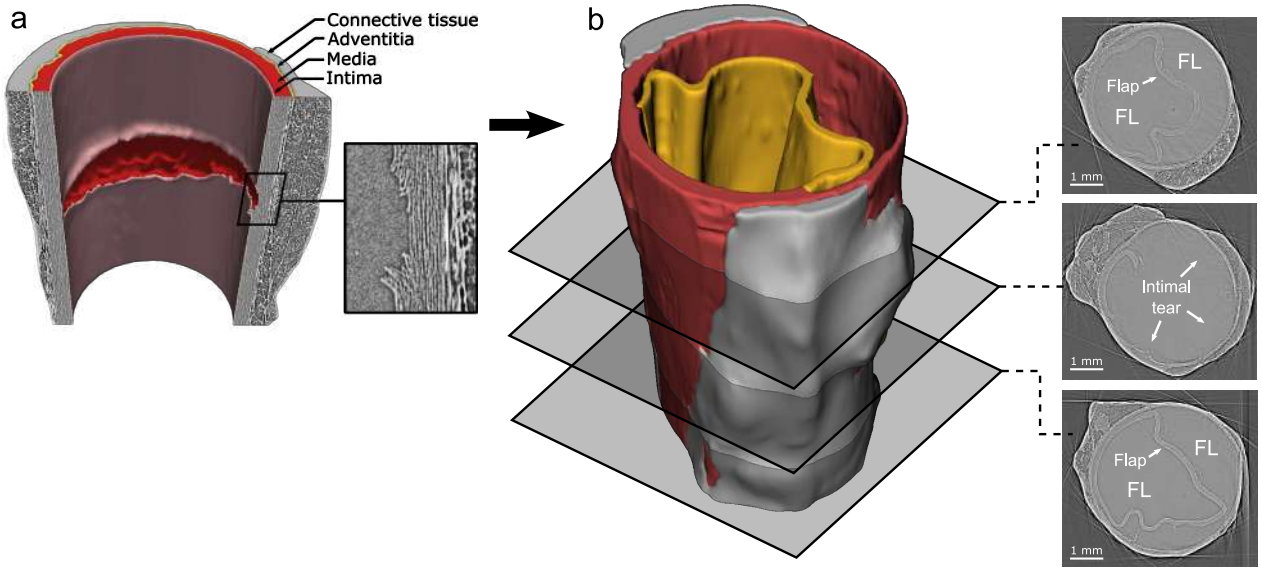

Figure 2: **Three-dimensional segmentation of a representative specimen with a circumferential notch after aortic dissection.** (**a**), 3D view of the specimen at 0 mmHg with the initial notch visible. (**b**), 3D view of the dissected sample at 0 mmHg. Three cross-sections are displayed at different locations along the longitudinal axis. The dissected flap is represented in yellow.

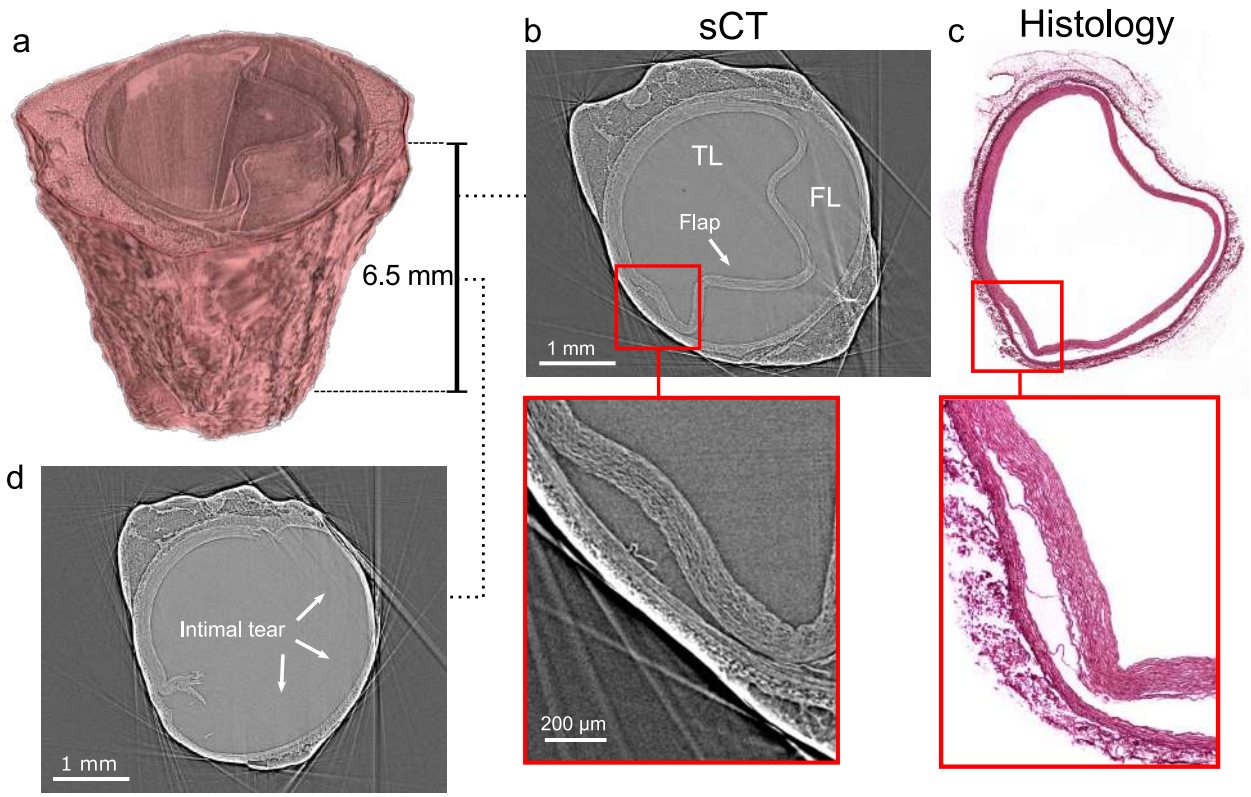

Figure 3: **Comparison of sCT and histology images of a dissected descending aorta.** The specimen was imaged after complete dissection, at a pressure of 0 mmHg. The critical pressure was 251 mmHg. **(a)**, 3D view of the dissected aorta. **(b)**, Cross-section with the dissected flap shown with a white arrow. TL: True lumen; FL: False lumen. **(c)**, Histology section in approximately the same location as **b**. The differences in morphology are due to the transportation and histological preparation. Sirius red staining, 5 µm-thick sections. Original magnification 4 ×. **(d)**, Cross-section showing the intimal tear.

3.3 Quantification of the morphology of the notch during inflation and correlation with the critical pressure

The evolution of the notch morphology is presented in Figure 4a,b,c. The length, width, and depth of the notch at 0 mmHg, after application of the pre-stretch, were 2.05 ± 1.75 mm, 113.5 ± 63.3°, 59.85 ± 18.52 % (Mean ± SD, n = 11), respectively. The notch dimensions remain mostly constant during the inflation of the aortic samples. These observations confirmed that the morphology of the notch follows the geometry of the aortic wall as observed in Brunet et al. [24]. The critical pressure as a function of the notch depth, the dissection length, and the notch width are presented in Figure 4d,e,f. The critical pressure was significantly correlated with the notch depth and dissection length ($p<0.05$), but not with notch width; the r^2 were 0.82, 0.38 and 0.29, respectively. These linear relations should be interpreted with caution as they were calculated with only 11 points (9 points for the circumferential notch and 2 points for the longitudinal notch).

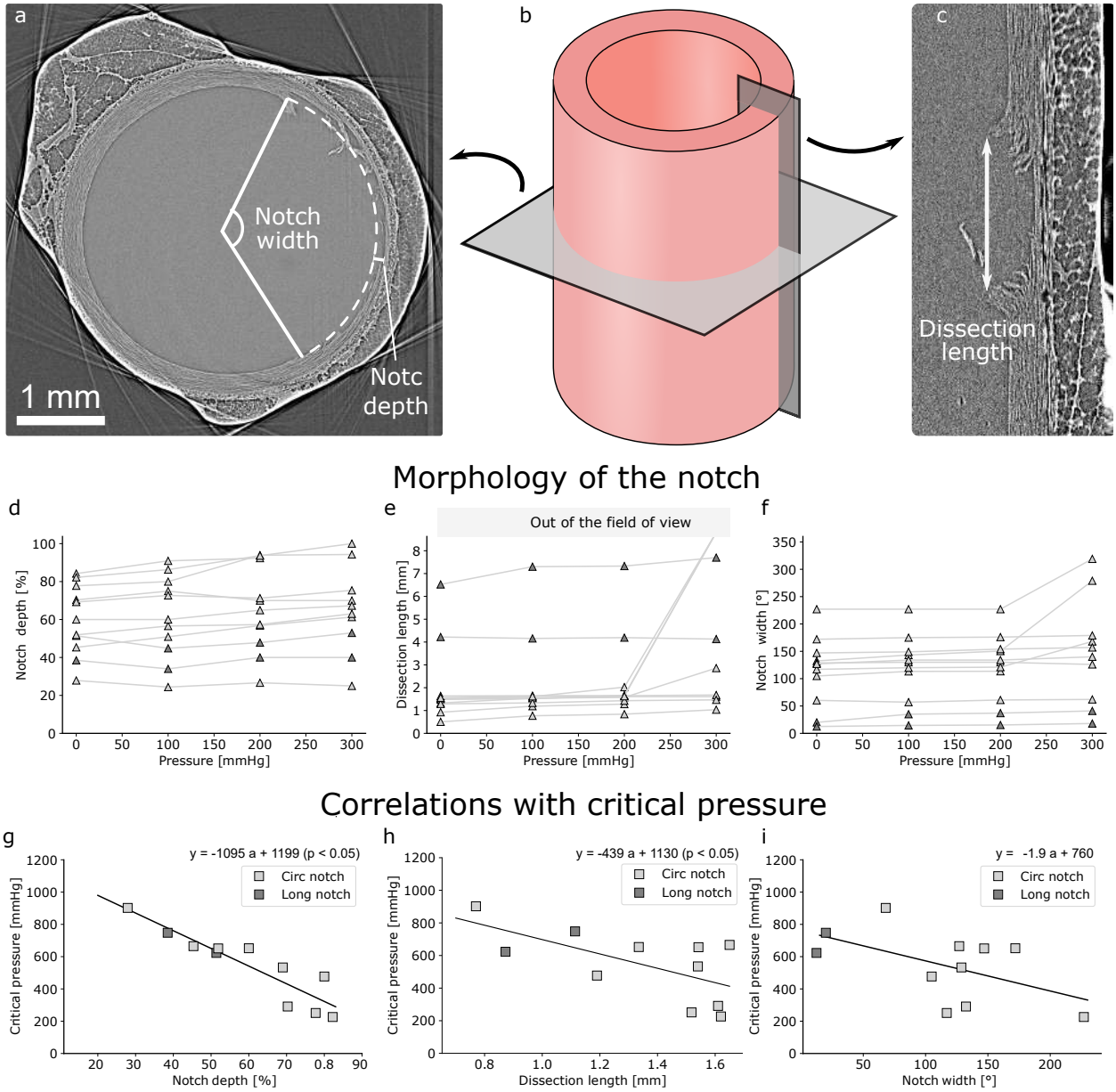

Figure 4: **Quantification of the morphology of the notch and correlations with critical pressure**. (**a**), cross-section of the aorta with indications on how the notch depth and notch width were calculated. (**b**), 3D schematics showing the orientation of (**a**) and (**c**). (**c**), longitudinal view of the aorta with the notch and indication on how is calculated the dissection length. (**d**) The notch depth, (**e**) the notch width, and (**f**) the notch length were plotted as a function of the pressure for each sample. Samples with a circumferential and longitudinal notch were differentiated. The critical pressures required to propagate the circumferential and longitudinal notches were plotted as a function of (**g**) the notch depth measured at 0 mmHg, and (**h**) the dissection length measured at 0 mmHg, and (**i**) the notch width measured at 0 mmHg. The notch depth was normalized with the medial thickness to obtain a percentage, a value of 0 corresponds to the medial side, whereas a value of 100 indicates a notch cutting the entire aortic wall from the intimal to the adventitial side. The lines represent the correlation found between the two variables. The r^2 of (**g**), (**h**), and (**i**) were 0.82, 0.38 and 0.29 respectively. Only the correlations critical pressure - notch depth and critical pressure - dissection length were found to be significant ($p < 0.05$).

3.4 Quantification of the morphology of the aorta during inflation

The inner diameter of the specimen before applying the pre-stretch was 4.21± 0.48 mm (n = 11). Manual measurements of diameters and thicknesses revealed a marked increase in the inner and outer diameter before reaching a plateau around 100 mmHg, while medial and adventitial thicknesses decreased with pressure (Figure 5). Furthermore, the thickness before and after propagation of the notch (at 0 mmHg) were compared with a paired t-test and it appears that the thickness after dissection is significantly lower ($p < 0.001$), indicating inelastic effects. The thickness was measured far from the failed part of the aorta to avoid local effect induced by the dissection. No statistical differences were found between the measurements on the cCT and sCT images. The number of medial lamellae measured on the sCT scans was in a range of 17 to 22. These measurements are similar to the values found by Wolinsky and Glagov on rabbits [27]. The mean circumferential Cauchy stress in the aortic specimens is plotted as a function of the pressure and stretch in Figure 5d,e.

As observed and quantified by Holzapfel et al. [36] a complex 3D residual stress is present in the unloaded arterial segment. As a consequence, the intimal flap shortens or extends once separated from the outer wall due to the release of residual stresses [37]. Two opposed mechanisms were observed: if the thickness of the flap is large (i.e. $> 50\%$ of the wall thickness), it shrinks by 5.3 – 26.1% once separated from the outer wall. Conversely, if the thickness of the flap is low (i.e. $< 50\%$ of the wall thickness), it extends from 3.8% to 13.6% once separated from the outer wall. This phenomenon was confirmed by histology. This caused a partial collapse of the flap and in some cases, a complete obstruction of the true lumen.

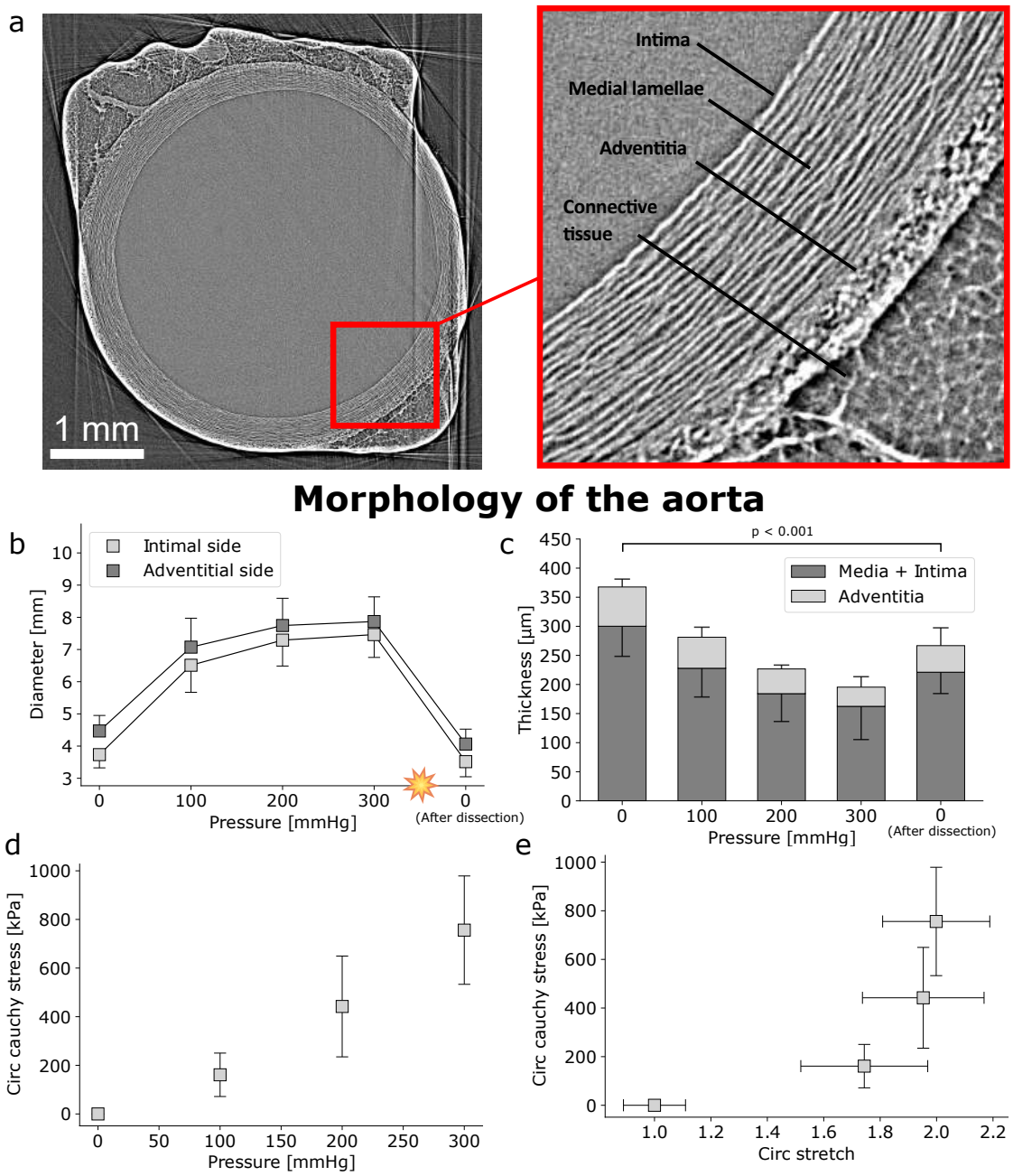

Figure 5: **Quantification of the morphology of the aortic wall**. (**a**), Cross-section of an aortic sample scanned by sCT, with a detail on the different architectural layers in the wall. (**b**) Inner and outer diameter of the aortic wall (mean values and standard deviations) as a function of the pressure. (**c**), Evolution of the intimal-medial and adventitial thicknesses (mean values and standard deviations) at each pressure steps and after propagation of the notch. The thicknesses were measured far from the notch. The thickness of the aortic wall was found to be significantly ($p < 0.001$) different after dissection compared to before. (**d**), (**e**), The circumferential Cauchy stress as a function of the pressure and the stretch.

3.5 Initiation mechanisms behind dissection

A front view with a focus on the notch area at different pressures and after propagation of the notch is presented in Figure 6b. A dissection propagated a first time at 251 mmHg, and a second time at 395 mmHg (Figure 6c), the first dissection only being detected during the post-processing of the data and was taken as the critical pressure. Figure 6b shows that the circumferential notch changed direction at 100 mmHg and initiated the dissection between the medial lamellae in the longitudinal direction. The dissection was extended longitudinally at 200 mmHg and propagated at 251 mmHg to the distal portion of the sample. Another example imaged by cCT may be observed in Supplementary Figure S1b.

In addition, it was observed at the notch site that the pressure was deforming the aortic wall, creating a bulge shape before and after propagation of the dissection. This bulge can be observed before dissection in Figure 6b where the aortic wall is straight at 0 mmHg and curved at 200 mmHg. It can also be observed on dissected specimens, for instance in Figure 3d or in Supplementary Figure S1a, in the middle cross-section. This mechanism is associated with a reduced radius of curvature of the undissected part of the wall around the notch site.

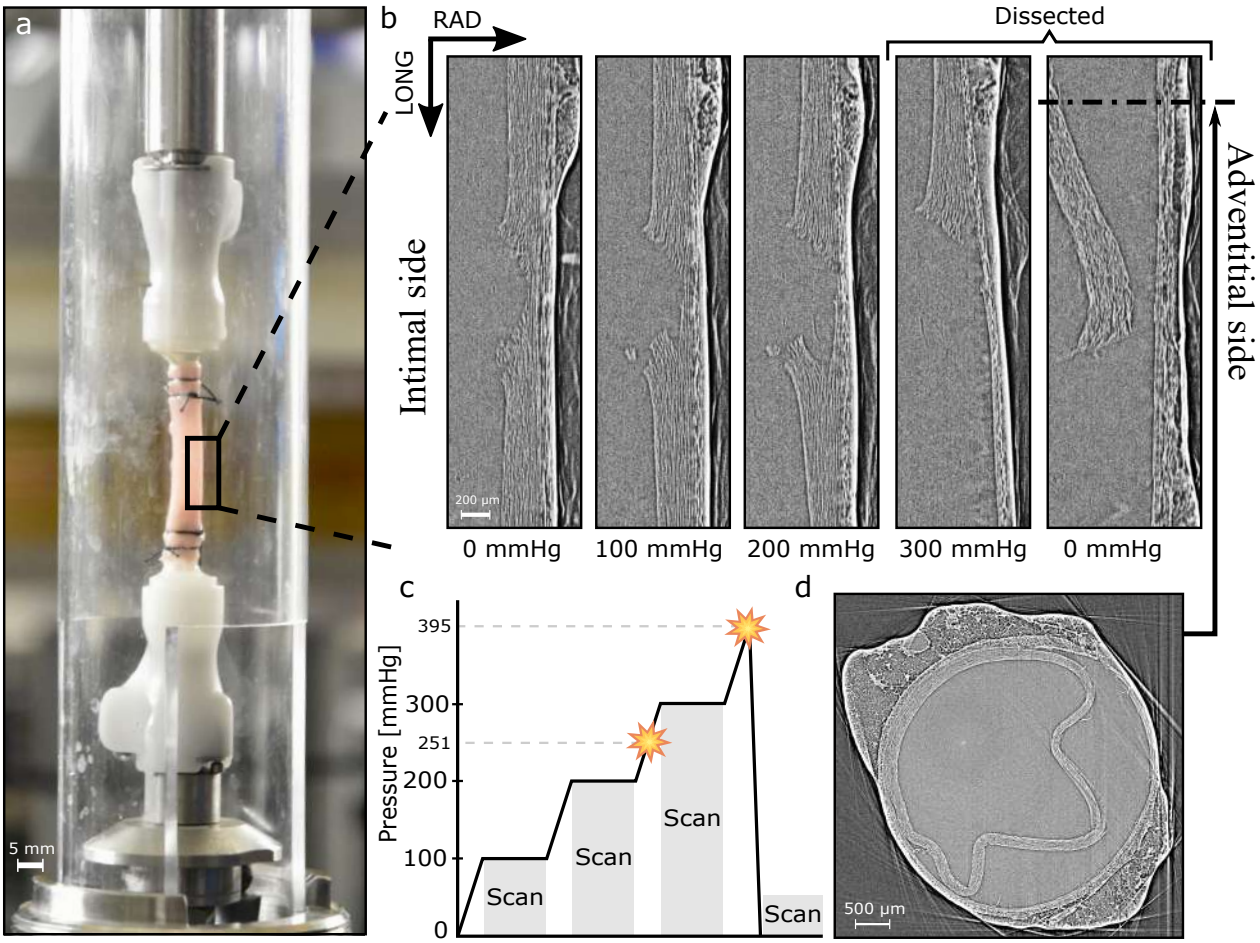

Figure 6: **Follow-up of a notched specimen at different pressure steps until dissection with ultra-high-resolution sCT.** (**a**), Rabbit descending aorta with a circumferential notch, sutured to the hydraulic connectors, during pressurization, in the transparent tube. The top of the specimen is the proximal side of the descending aorta. (**b**), Front view of the aortic wall with a focus on the notch at different pressures and after propagation of the dissection along the aorta. The intimal side is on the left whereas the adventitial side is on the right. The upper part is the proximal side while the lower part is the distal side. (**c**), The different steps of pressure applied to the sample. As shown in (**b**), the notch propagated distally at 251 mmHg and proximally at 395 mmHg. The first dissection was only detected during the post-processing of the data. (**d**), Cross-section of the sample at 0 mmHg after dissection with the intimal flap dissected from the outer wall.

3.6 Real-time visualization of the dissection propagation

The dissection of the aortic segments was captured in real-time with conventional radiography and synchrotron radiography. A video of a complete dissection in real-time is presented in Supplementary Materials (Supplementary Video 2). The dissection of the specimens which propagated before 300 mmHg could not be captured. Furthermore, the samples with a longitudinal notch were not visualized with radiographic images as the notch orientation hindered the observation with this type of technique. An example of the follow-up in real-time of a dissection is presented in Figure 7a at different time steps. In this study, the complete propagation of the notch along the aorta occurred in 10.3 $\pm$ 2.5 s (n = 6). As presented in Figure 7, three

stages could be observed: (1) The notch followed the deformation of the aortic wall but the dissection was not yet initiated, (2) after the initiation of the dissection, the notch propagated at a slow rate. The average dissection rate during this step was 0.23 ± 0.04 mm/s (n = 6). In the last step (3), the sample dissected entirely quasi-instantaneously (in 2–5s) and a rupture of the false lumen caused the pressure to drop. The dissection rate could not be calculated during this step because the frame rate and the field of view were not sufficient to capture the propagation.

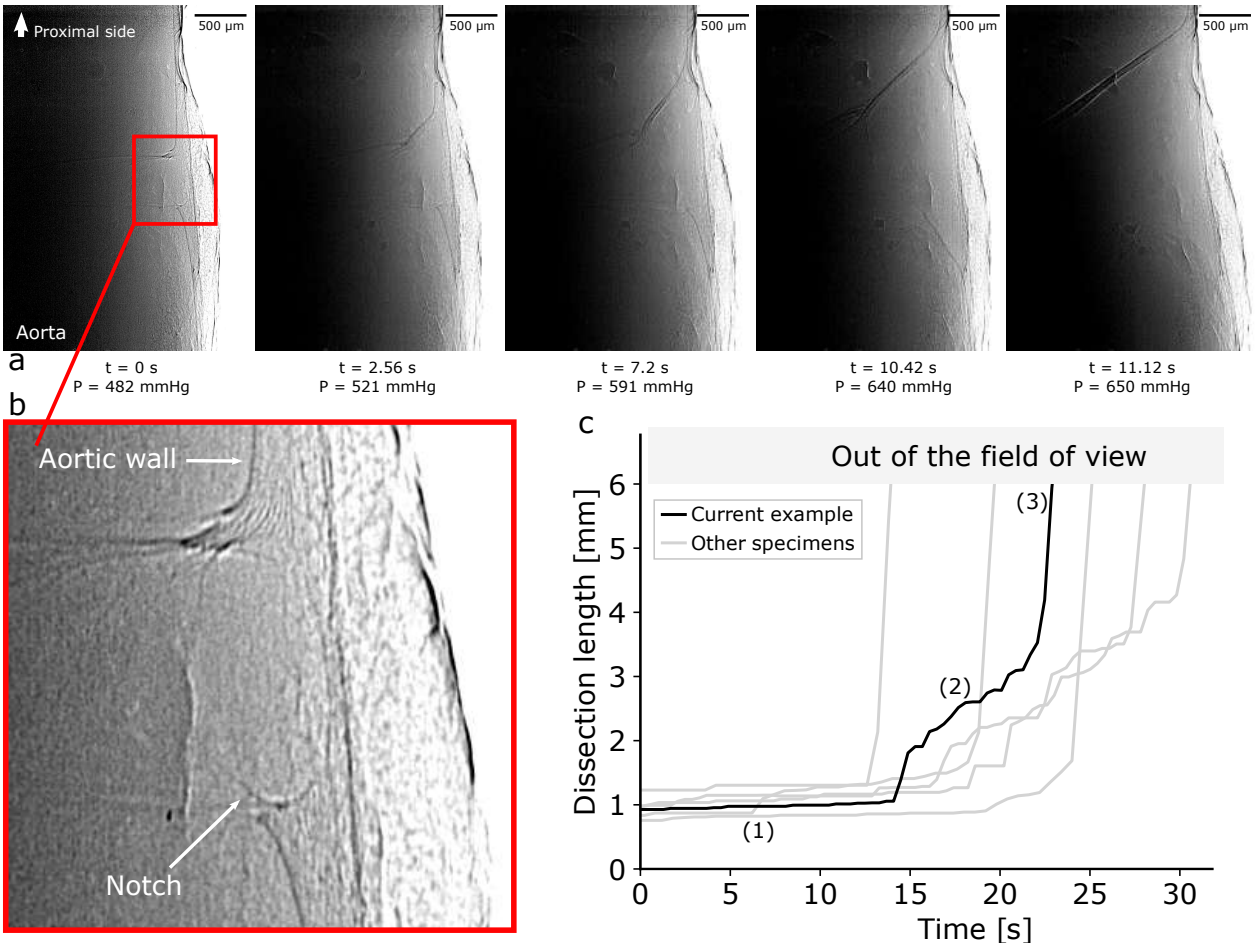

Figure 7: **Real-time visualization of the propagation of the dissection in the aortic wall.** (**a**), 2D radiographic front view of the dissection propagation along the aorta at different time steps. To begin with, the notch propagated toward the proximal side of the sample on few millimeters (3.9 mm), at the same time, the specimen was delaminated entirely from the notch to the connector in the distal direction. The complete video of the dissection is available in Supplementary Materials (Supplementary Video 2). (**b**), Close-up of the notch before propagation. (**c**), Dissection length as a function of the time for all samples with a circumferential notch (except for specimens that have dissected before 300 mmHg). The black curve corresponds to the sample presented in (**a**). Three steps were observed: (1) the notch was deformed with the aortic wall but the dissection was not yet initiated, (2) a local propagation of the dissection started at a slow rate, (3) before propagating almost instantaneously to the entire sample. The measurements were taken manually and stopped when the dissection extended outside the field of view.

4 Discussion

In this study, an in situ tension-inflation test was performed on notched rabbit aortic segments until dissection of the sample. The mechanical test was imaged with cCT and sCT at different steps of pressure and in real-time to observe the evolution of the notch morphology, the aortic geometry, and their influence on critical pressure, initiation, and propagation of the dissection. To the authors' knowledge, this is the first study to observe the complete aortic dissection process with the entire 3D aortic geometry and a resolution allowing quantification of microstructural metrics. It is also the first time that an aortic dissection is observed in real-time. Our methodology bridges the gap between mechanics of the aorta at a global and micro scale allowing the microstructural changes underlying the dissection process to be investigated.

4.1 Comparison with other experimental dissection models

The peak pressures required to propagate a notch were mostly non-physiological, and a deep and wide notch was necessary to reach dissection of the vessel within a physiological blood pressure range. This confirms the presence of a medial degeneration prior to the development of an aortic dissection as observed in literature [5, 38]. The values of critical pressures found in this study are coherent with literature [13, 38–40]. The negative correlation between the notch depth and critical pressure observed in this study is also in agreement with the literature [14, 41]. Peelukhana et al. [41] used a pulse duplication device to study the effect of different geometric parameters on aortic dissection propagation in porcine aortas with a single-entry tear, demonstrating that a deeper notch is more likely to propagate than a shallow notch for the same pressure. However, further comparison seems difficult as the tissues and methods are different.

4.2 Aortic dissection sequence

The aortic dissection can be divided into three stages: (i) a pre-existing defect (the notch here) initiates the propagation in the radial direction of the aortic wall up to the outer half of the media [15, 42, 43], while the blood pressure deforms the notch and the aortic wall, (ii) the crack shifts in direction towards an interlamellar propagation in the media (circumferential-longitudinal plane) due to the high shear stress at the tip of the notch and to the low failure strength between the lamellae compared to other directions [44], and finally (iii) the blood penetrates through the crack between the lamellae and delaminates the aorta. These different steps are presented in Figure 8. In this study, we investigated steps (ii) and (iii).

4.3 Creation of the initial defect

In the scientific community, the initial weak spot in the media (step (i)) is considered to be the consequence of a medial degeneration, due to aging or an inherited connective tissue disorder [4]. This phenomenon would be difficult to model experimentally, hence the manual creation of a notch in the present study to initiate the dissection. In some patients, only step (i) and eventually step (ii) is achieved, with the crack never propagating, thus forming an abortive, discrete dissection, also called incomplete dissection [45–48].

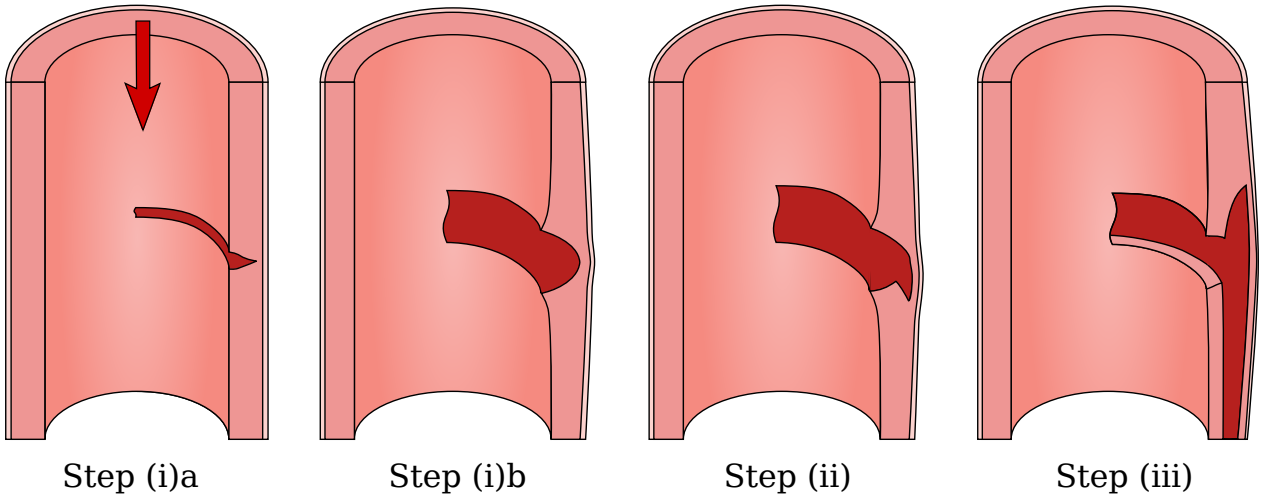

Figure 8: **Schematic describing the steps of aortic dissection as observed in these experiments. (i)a** an initial notch propagates to the outer media, while **(i)b** the blood pressure deforms the notch and the aortic wall, creating a bulge, **(ii)** the crack changes of direction due to the laminated structure of the medial layer and the high shear stress at the tip of the notch, and **(iii)** the blood enters between the lamellae and pushes them apart. The arrow shows the direction of the blood flow.

4.4 Shift of the crack towards interlamellar propagation

The change of direction of the crack to an interlamellar propagation (step (ii)) is due to a combination of factors: the low interlamellar cohesion compared to the translamellar strength of the aortic wall being one of them. [44, 49].

The shear stress imposed on the aortic wall is also increasingly believed by the research community to play a key role in the initiation of the dissection [12, 50–53]. The cross-section of the notch in Figure 6 showing an open crack indicates the presence of shear stress at the tip of the notch due to the axial physiological stretch and the fluid pressure applied on the wall. In the literature, some studies have investigated this mechanism by inflating notched bovine aortic rings [51] or by using lap-shear testing on notched sheep aortic samples [52]; nevertheless, these experiments were far from in vivo condition and only the propagation of a longitudinal notch was investigated, whereas 80 % to 95 % of clinically observed intimal tears are circumferential [2,54,55].

Another consequence of the fluid pressure is the deformation of the adventitia and remaining media, forming an eccentric bulge at the tip of the notch as shown in Figure 6b, S1b, and 7. This change in the aortic morphology is often observed in clinics on patient with discrete aortic dissection [46, 56, 57]. The negative correlation of the notch depth with the critical pressure (Figure 4) is also confirmed by clinical observations where most dissections propagate into the outer half of the aortic wall [15, 42, 43, 55].

4.5 Delamination of the aorta

Finally, in step (iii), once the interlamellar propagation of the notch begins, the blood enters between the lamellae, presumably adding crack opening stress (stress at which the crack surfaces open) in addition to the shear stress (Figure 8). According to the real-time visualization (Figure 7 and Supplementary Video 2), the dissection occurred in about 10 seconds from initiation to complete propagation. This is consistent with clinical observations which stated that aortic dissection occurs in only a few seconds [15]. It is likely that the mechanisms involved during this step are similar to those observed in intramural liquid infusion [14] or peeling testing [10], i.e. predominantly tension fracture. The finding that aortic dissection propagates along the aorta in the longitudinal direction, mostly involving about half the circumference of the aorta is also consistent with clinical observations [43, 45, 58]. In addition, the release of residual stress and the elastic recoil of the detached flap leads to a collapse of the flap and increases the stress concentration at the crack front. These mechanisms create a chain reaction that propagates the dissection along the aorta until this process is interrupted, for instance, by an atherosclerosis plaque [15, 55, 59], a branch (as observed in Supplementary Figure S3), a re-entry tear, or a rupture of the outer wall.

4.6 The particular case of longitudinal notches

The phenomena previously described (i.e. change of aortic morphology and bulge effect) were not observed on samples with a longitudinal notch as shown in Supplementary Figure S2 by sample III. The fact that the notch depths of the two longitudinally notched specimens were small compared to the well-dissected samples could be an explanation. The pressure required to dissect a specimen with a circumferential notch was lower than for a specimen with a longitudinal notch; however, the difference in geometry of the notches and the small number of samples prevent a definitive conclusion from being reached. In addition, both longitudinally notched specimens seem to follow the same trends observed on circumferentially notched specimens in terms of correlation with notch morphological factors, such as depth of notch (Figure 4). Thus, the prevalence of circumferential notch observed in clinics may be due mainly to the lower resistance of aortic tissue to longitudinal versus circumferential tension, as shown by Witzenburg et al. [44] using uniaxial testing on

porcine ascending aortic samples.

4.7 Limitations and future work

Some limitations to this study should be noted. Freezing samples prior to testing could affect the mechanical properties; however, the extent of this effect is still under debate in the scientific community [60–62]. Further investigation is needed to quantify the influence of freezing on the dissection of such specimens. The small number of samples is also a limitation of this study, as it prevents definitive conclusions from being drawn, for instance on the differences between circumferential and longitudinal notches. Under in vivo conditions, the aorta is subjected to dynamic loading, but the tension-inflation test was performed at static pressure, which may be the reason for the non-physiological pressure necessary to propagate the notch, as in literature $(\frac{dP}{dt})_{\max}$ was shown to have a significant influence on the critical pressure compared to the mean pressure [63, 64]. Further studies, with a dynamic load closer to in vivo conditions, are required to quantify the influence of this parameter on the initiation of aortic dissection. The fact that young rabbits were used as an animal model may explain that the measured critical pressures were well above physiological range, and also dictated the need to initiate the dissection manually due to the lack of pre-existing intramural defects. Genetically-modified mouse models could be used in future works as a more physiological model of the diseased state of the wall [26]. Nevertheless, the methodology we have developed allowed a detailed characterization and understanding of this condition, both on a macro- and micro-scale. Finally, the data reported in this study could be of great use in computational modelling by filling the lack of experimental data in literature and enabling future aortic dissection models to be validated [65].

Data availability

The complete data, of considerable size, generated and analyzed in the current study are available from the corresponding authors upon reasonable request.

Competing interests

The authors declare no competing interests.

Author contributions

Conception and design of the study: J.B., P.B., B.P., N.C, and B.L. Acquisition of data: J.B., J.A., B.P., N.C., and A.B. Histology: N.L. Interpretation of data, revision of the manuscript, final approval and agreement to be accountable for all aspects of the work: all authors. Drafting of the manuscript: J.B. and B.P.

Acknowledgement

The authors would like to thank the ESRF for the provision of the beamtime, the ID17 beamline staff for their helpful scientific and technical support, and the Bergerie de la Combe au Loup (Boisset-Saint-Priest, France) for providing the rabbit aortas used in this study. This work was supported by the European Research Council through Starting Grant AArteMIS n°638804.

References

[1] Christoph A Nienaber, Rachel E Clough, Natzi Sakalihasan, Toru Suzuki, Richard Gibbs, Firas Mussa, Michael P Jenkins, Matt M Thompson, Arturo Evangelista, James SM Yeh, et al. Aortic dissection. *Nat. Rev. Dis. Primers.*, 2(1):1–18, 2016.

[2] MJ Thubrikar, P Agali, and F Robicsek. Wall stress as a possible mechanism for the development of transverse intimal tears in aortic dissections. *J. Med. Eng. Technol.*, 23(4):127–134, 1999.

[3] Hiroaki Osada, Masahisa Kyogoku, Motonori Ishidou, Manabu Morishima, and Hiroyuki Nakajima. Aortic dissection in the outer third of the media: what is the role of the vasa vasorum in the triggering process? *Eur. J. Cardio-Thorac. Surg.*, 43(3):e82–e88, 2012.

[4] Christoph A Nienaber and Rachel E Clough. Management of acute aortic dissection. *The Lancet*, 385(9970):800–811, 2015.

[5] Yutaka Nakashima. Pathogenesis of aortic dissection: elastic fiber abnormalities and aortic medial weakness. *Annals of vascular diseases*, 3(1):28–36, 2010.

[6] Ashkan Karimi and Dianna M Milewicz. Structure of the elastin-contractile units in the thoracic aorta and how genes that cause thoracic aortic aneurysms and dissections disrupt this structure. *Canadian Journal of Cardiology*, 32(1):26–34, 2016.

[7] D Weiss, M Latorre, BV Rego, C Cavinato, BJ Tanski, AG Berman, CJ Goergen, and JD Humphrey. Biomechanical consequences of compromised elastic fiber integrity and matrix cross-linking on abdominal aortic aneurysmal enlargement. *Acta Biomaterialia*, 134:422–434, 2021.

[8] Toshiharu Ishii and Noriko Asuwa. Collagen and elastin degradation by matrix metalloproteinases and tissue inhibitors of matrix metalloproteinase in aortic dissection. *Human pathology*, 31(6):640–646, 2000.

[9] Dianna M Milewicz, Kathleen M Trybus, Dong-chuan Guo, H Lee Sweeney, Ellen Regalado, Kristine Kamm, and James T Stull. Altered smooth muscle cell force generation as a driver of thoracic aortic aneurysms and dissections. *Arteriosclerosis, thrombosis, and vascular biology*, 37(1):26–34, 2017.

[10] Gerhard Sommer, T Christian Gasser, Peter Regitnig, Martin Auer, and Gerhard A Holzapfel. Dissection properties of the human aortic media: an experimental study. *J. Biomech. Eng.*, 130(2):021007, 2008.

[11] Christopher Noble, Nicole Smulders, Roger Lewis, Matt J Carré, Steve E Franklin, Sheila MacNeil, and Zeike A Taylor. Controlled peel testing of a model tissue for diseased aorta. *J. Biomech.*, 49(15):3667–3675, 2016.

[12] Gerhard Sommer, Selda Sherifova, Peter J Oberwalder, Otto E Dapunt, Patricia A Ursomanno, Abe DeAnda, Boyce E Griffith, and Gerhard A Holzapfel. Mechanical strength of aneurysmatic and dissected human thoracic aortas at different shear loading modes. *J. Biomech.*, 49(12):2374–2382, 2016.

[13] Michael W Carson and Margot R Roach. The strength of the aortic media and its role in the propagation of aortic dissection. *J. Biomech.*, 23(6):579–588, 1990.

[14] Amy SM Tam, M Catherine Sapp, and Margot R Roach. The effect of tear depth on the propagation of aortic dissections in isolated porcine thoracic aorta. *J. Biomech.*, 31(7):673–676, 1998.

[15] William C Roberts. Aortic dissection: anatomy, consequences, and causes. *American heart journal*, 101(2):195–214, 1981.

[16] Joseph Brunet, Baptiste Pierrat, and Pierre Badel. Review of current advances in the mechanical description and quantification of aortic dissection mechanisms. *IEEE Rev. Biomed. Eng.*, 2020.

[17] Mary K O'Connell, Sushila Murthy, Samson Phan, Chengpei Xu, JoAnn Buchanan, Ryan Spilker, Ronald L Dalman, Christopher K Zarins, Winfried Denk, and Charles A Taylor. The three-dimensional micro-and nanostructure of the aortic medial lamellar unit measured using 3D confocal and electron microscopy imaging. *Matrix Biol.*, 27(3):171–181, 2008.

[18] M Di Giuseppe, M Zingales, S Pasta, and S Avril. In vitro measurement of strain localization preceding dissection of the aortic wall subjected to radial tension. *Experimental Mechanics*, 61(1):119–130, 2021.

[19] Will Goth, John Lesicko, Michael S. Sacks, and James W. Tunnell. Optical-Based Analysis of Soft Tissue Structures. *Annu. Rev. Biomed. Eng.*, 18(1):357–385, July 2016.

[20] Cristina Cavinato, Clementine Helfenstein-Didier, Thomas Olivier, Sabine Rolland Du Roscoat, Norbert Laroche, and Pierre Badel. Biaxial loading of arterial tissues with 3d in situ observations of adventitia fibrous microstructure: a method coupling multi-photon confocal microscopy and bulge inflation test. *J. Mech. Behav. Biomed. Mater.*, 74:488–498, 2017.

[21] Xunjie Yu, Béla Suki, and Yanhang Zhang. Avalanches and power law behavior in aortic dissection propagation. *Science advances*, 6(21):eaaz1173, 2020.

[22] Bram Trachet, Rodrigo A Fraga-Silva, Francisco J Londono, Abigaíl Swillens, Nikolaos Stergiopulos, and Patrick Segers. Performance comparison of ultrasound-based methods to assess aortic diameter and stiffness in normal and aneurysmal mice. *PLoS One*, 10(5):e0129007, 2015.

[23] Clémentine Helfenstein-Didier, Damien Taïnoff, Julien Viville, Jérôme Adrien, Eric Maire, and Pierre Badel. Tensile rupture of medial arterial tissue studied by x-ray micro-tomography on stained samples. *J. Mech. Behav. Biomed. Mater.*, 78:362–368, 2018.

[24] J Brunet, B Pierrat, J Adrien, E Maire, N Curt, and P Badel. A novel method for in vitro 3d imaging of dissecting pressurized arterial segments using x-ray microtomography. *Exp. Mech.*, pages 1–11, 2020.

[25] Bram Trachet, Mauro Ferraro, Goran Lovric, Lydia Aslanidou, Gerlinde Logghe, Patrick Segers, and Nikolaos Stergiopulos. Synchrotron-based visualization and segmentation of elastic lamellae in the mouse carotid artery during quasi-static pressure inflation. *J. R. Soc. Interface*, 16(155):20190179, 2019.

[26] Gerlinde Logghe, Bram Trachet, Lydia Aslanidou, Pablo Villaneuva-erez, Julie De Backer, Nikolaos Stergiopulos, Marco Stampanoni, Hiroki Aoki, and Patrick Segers. Propagation-based phase-contrast synchrotron imaging of aortic dissection in mice: from individual elastic lamella to 3d analysis. *Scientific Reports*, 8(1):1–11, 2018.

[27] Harvey Wolinsky and Seymour Glagov. A lamellar unit of aortic medial structure and function in mammals. *Circ. Res.*, 20(1):99–111, 1967.

[28] Sulagna Dutta and Pallav Sengupta. Rabbits and men: relating their ages. *Journal of basic and clinical physiology and pharmacology*, 29(5):427–435, 2018.

[29] J-Y Buffiere, E Maire, J Adrien, J-P Masse, and E Boller. In situ experiments with x ray tomography: an attractive tool for experimental mechanics. *Experimental mechanics*, 50(3):289–305, 2010.

[30] David Paganin, Sheridan C Mayo, Tim E Gureyev, Peter R Miller, and Steve W Wilkins. Simultaneous phase and amplitude extraction from a single defocused image of a homogeneous object. *Journal of microscopy*, 206(1):33–40, 2002.

[31] Johannes Schindelin, Ignacio Arganda-Carreras, Erwin Frise, Verena Kaynig, Mark Longair, Tobias Pietzsch, Stephan Preibisch, Curtis Rueden, Stephan Saalfeld, Benjamin Schmid, et al. Fiji: an open-source platform for biological-image analysis. *Nature methods*, 9(7):676–682, 2012.

[32] Curtis T Rueden, Johannes Schindelin, Mark C Hiner, Barry E DeZonia, Alison E Walter, Ellen T Arena, and Kevin W Eliceiri. Imagej2: Imagej for the next generation of scientific image data. *BMC bioinformatics*, 18(1):529, 2017.

[33] Andriy Fedorov, Reinhard Beichel, Jayashree Kalpathy-Cramer, Julien Finet, Jean-Christophe Fillion-Robin, Sonia Pujol, Christian Bauer, Dominique Jennings, Fiona Fennessy, Milan Sonka, et al. 3d slicer as an image computing platform for the quantitative imaging network. *Magnetic resonance imaging*, 30(9):1323–1341, 2012.

[34] Amy Henderson Squillacote, James Ahrens, Charles Law, Berk Geveci, Kenneth Moreland, and Brad King. *The paraview guide*, volume 366. Kitware Clifton Park, NY, 2007.

[35] Charles S Roberts and William C Roberts. Aortic dissection with the entrance tear in the descending thoracic aorta. analysis of 40 necropsy patients. *Annals of surgery*, 213(4):356, 1991.

[36] Gerhard A Holzapfel, Gerhard Sommer, Martin Auer, Peter Regitnig, and Ray W Ogden. Layer-specific 3d residual deformations of human aortas with non-atherosclerotic intimal thickening. *Ann. Biomed. Eng.*, 35(4):530–545, 2007.

[37] David M Williams, Mark A LePage, and Do Yun Lee. The dissected aorta: part i. early anatomic changes in an in vitro model. *Radiology*, 203(1):23–31, 1997.

[38] IM Tiessen and MR Roach. Factors in the initiation and propagation of aortic dissections in human autopsy aortas. *J. Biomech. Eng.*, 115(1):123–125, 1993.

[39] Albert E Hirst Jr and Varner J Johns Jr. Experimental dissection of media of aorta by pressure: its relation to spontaneous dissecting aneurysm. *Circ. Res.*, 10(6):897–903, 1962.

[40] Margot R Roach and SH Song. Variations in strength of the porcine aorta as a function of location. *Clin. Invest. Med.*, 17(4):308, 1994.

[41] Srikara V Peelukhana, Yanmin Wang, Zachary Berwick, Jarin Kratzberg, Joshua Krieger, Blayne Roeder, Rachel E Cloughs, Albert Hsiao, Sean Chambers, and Ghassan S Kassab. Role of pulse pressure and geometry of primary entry tear in acute type b dissection propagation. *Ann. Biomed. Eng.*, 45(3):592–603, 2017.

[42] Hiroaki Osada, Masahisa Kyogoku, Motonori Ishidou, Manabu Morishima, and Hiroyuki Nakajima. Aortic dissection in the outer third of the media: what is the role of the vasa vasorum in the triggering process? *Eur. J. Cardiothorac. Surg.*, 43(3):e82–e88, March 2013.

[43] Mano J Thubrikar. *Vascular mechanics and pathology*, volume 494. Springer, 2007.

[44] Colleen M Witzenburg, Rohit Y Dhume, Sachin B Shah, Christopher E Korenczuk, Hallie P Wagner, Patrick W Alford, and Victor H Barocas. Failure of the porcine ascending aorta: multidirectional experiments and a unifying microstructural model. *J. Biomech. Eng.*, 139(3), 2017.

[45] Charles A Murray and Jesse E Edwards. Spontaneous laceration of ascending aorta. *Circulation*, 47(4):848–858, 1973.

[46] Lars G Svensson, Sherif B Labib, Andrew C Eisenhauer, and John R Butterly. Intimal tear without hematoma: an important variant of aortic dissection that can elude current imaging techniques. *Circulation*, 99(10):1331–1336, 1999.

[47] R Erbel, F Alfonso, C Boileau, O Dirsch, B Eber, A Haverich, H Rakowski, J Struyven, K Radegran, U Sechtem, et al. Diagnosis and management of aortic dissection: task force on aortic dissection, european society of cardiology. *European heart journal*, 22(18):1642–1681, 2001.

[48] Jae-Kwan Song. Update in acute aortic syndrome: intramural hematoma and incomplete dissection as new disease entities. *Journal of Cardiology*, 64(3):153–161, 2014.

[49] Ahmed Sayed, Malak Munir, and Eshak I Bahbah. Aortic dissection: a review of the pathophysiology, management and prospective advances. *Current Cardiology Reviews*, 17(4), 2021.

[50] Henry W Haslach Jr, Lauren N Leahy, Parinaz Fathi, Joshua M Barrett, Amanda E Heyes, Thomas A Dumsha, and Eileen L McMahon. Crack propagation and its shear mechanisms in the bovine descending aorta. *Cardiovasc. Eng. Technol.*, 6(4):501–518, 2015.

[51] Henry W Haslach Jr, Ahmed Siddiqui, Amanda Weerasooriya, Ryan Nguyen, Jacob Roshgadol, Noel Monforte, and Eileen McMahon. Fracture mechanics of shear crack propagation and dissection in the healthy bovine descending aortic media. *Acta Biomater.*, 68:53–66, 2018.

[52] Brian FitzGibbon and Patrick McGarry. Development of a test method to investigate mode ii fracture and dissection of arteries. *Acta Biomaterialia*, 2020.

[53] Joanna Gawinecka, Felix Schönrath, and Arnold von Eckardstein. Acute aortic dissection: pathogenesis, risk factors and diagnosis. *Swiss medical weekly*, 147:w14489, 2017.

[54] Artur Evangelista, Armando Salas, Aida Ribera, Ignacio Ferreira-González, Hug Cuellar, Victor Pineda, Teresa González-Alujas, Bart Bijnens, Gaietà Permanyer-Miralda, and David Garcia-Dorado. Long-term outcome of aortic dissection with patent false lumen: predictive role of entry tear size and location. *Circulation*, 125(25):3133–3141, 2012.

[55] William M Sherk, Minhaj S Khaja, and David M Williams. Anatomy, pathology, and classification of aortic dissection. *Techniques in Vascular and Interventional Radiology*, 24(2):100746, 2021.

[56] Anne S Chin, Martin J Willemink, Aya Kino, Virginia Hinostroza, Anna M Sailer, Michael P Fischbein, R Scott Mitchell, Gerald J Berry, D Craig Miller, and Dominik Fleischmann. Acute limited intimal tears of the thoracic aorta. *Journal of the American College of Cardiology*, 71(24):2773–2785, 2018.

[57] Raimund Erbel, Victor Aboyans, Catherine Boileau, Eduardo Bossone, Roberto Di Bartolomeo, Holger Eggebrecht, Arturo Evangelista, Volkmar Falk, Herbert Frank, et al. 2014 esc guidelines on the diagnosis and treatment of aortic diseases: document covering acute and chronic aortic diseases of the thoracic and abdominal aorta of the adult the task force for the diagnosis and treatment of aortic diseases of the european society of cardiology (esc). *European heart journal*, 35(41):2873–2926, 2014.

[58] Coumba Thiam, Boubacar Sonfo, Youssouf Camara, Souleymane Sanogo, Hamidou Oumar Bâ, Sidibé Samba, Massama Konaté, Asmaou Keita, Sako Mariam, Mahamadou Cissé, et al. Double emergency pulmonary embolism and aortic dissection: about a clinical case. *World Journal of Cardiovascular Diseases*, 10(08):550, 2020.

[59] Istvan Meszaros, Jozsef Morocz, Jozsef Szlavi, Janos Schmidt, Laszlo Tornoci, Laszlo Nagy, and Laszlo Szép. Epidemiology and clinicopathology of aortic dissection. *Chest*, 117(5):1271–1278, 2000.

[60] Brian D Stemper, Narayan Yoganandan, Michael R Stineman, Thomas A Gennarelli, Jamie L Baisden, and Frank A Pintar. Mechanics of fresh, refrigerated, and frozen arterial tissue. *Journal of Surgical Research*, 139(2):236–242, 2007.

[61] Jorge O Virues Delgadillo, Sebastien Delorme, Rouwayda El-Ayoubi, Robert DiRaddo, Savvas G Hatzikiriakos, et al. Effect of freezing on the passive mechanical properties of arterial samples. *Journal of Biomedical Science and Engineering*, 3(07):645, 2010.

[62] Siobhan A O'Leary, Barry J Doyle, and Tim M McGloughlin. The impact of long term freezing on the mechanical properties of porcine aortic tissue. *Journal of the mechanical behavior of biomedical materials*, 37:165–173, 2014.

[63] Edward K Prokop, Roger F Palmer, and Myron W Wheat Jr. Hydrodynamic forces in dissecting aneurysms: in-vitro studies in a tygon model and in dog aortas. *Circ. Res.*, 27(1):121–127, 1970.

[64] Charles van Baardwijk and Margot R Roach. Factors in the propagation of aortic dissections in canine thoracic aortas. *J. Biomech.*, 20(1):67–73, January 1987.

[65] Osman Gültekin, Sandra Priska Hager, Hüsnü Dal, and Gerhard A Holzapfel. Computational modeling of progressive damage and rupture in fibrous biological tissues: application to aortic dissection. *Biomech. Model. Mechanobiol.*, pages 1–22, 2019.

Supplementary Materials

Supplementary Video 1: Overview of the notched aorta at different pressure steps until dissection. Transverse slices of 5 scans (0 mmHg, 100 mmHg, 200 mmHg, 300 mmHg, and 0 mmHg after dissection) are shown. The pressure present inside the aorta is indicated on the top left corner. The aortic wall and intimal tear are indicated, as well as the false and true lumen after dissection. The isotropic voxel size is 3.02 µm.

Supplementary Video 2: Real-time aortic dissection recorded using radiographic images. The complete dissection of the sample can be observed when the critical pressure is reached. The dissection length follows an exponential curve as shown in Figure 7.

Visualization of the descending aorta with conventional computed tomographic

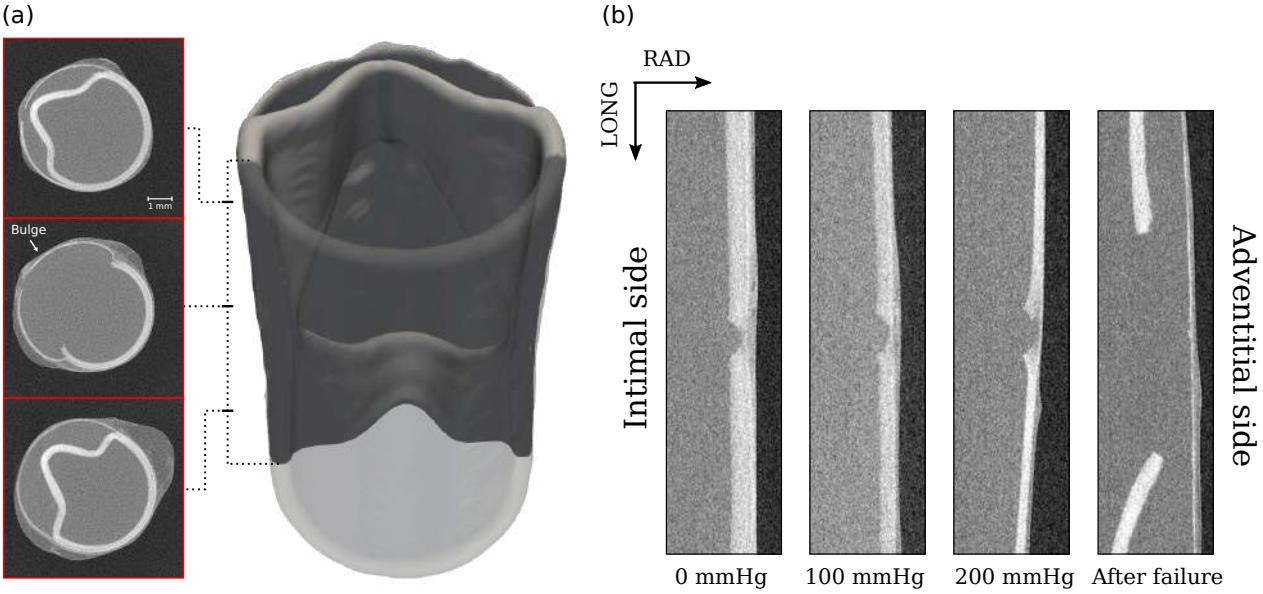

Figure S1: **(a)** Three-dimensional segmentation of a representative specimen with a circumferential notch after aortic dissection. Three cross-sections were displayed at different locations along the longitudinal axis. The length of the portion of the specimen observed here is 8.75 mm. The outer wall presents a bulge in the middle cross-section. **(b)** Front view of the aortic wall with a focus on the notch at different pressures and after propagation of the dissection along the aorta. The intimal side is on the left whereas the adventitial side is on the right. The sample dissected at a critical pressure of 477 mmHg

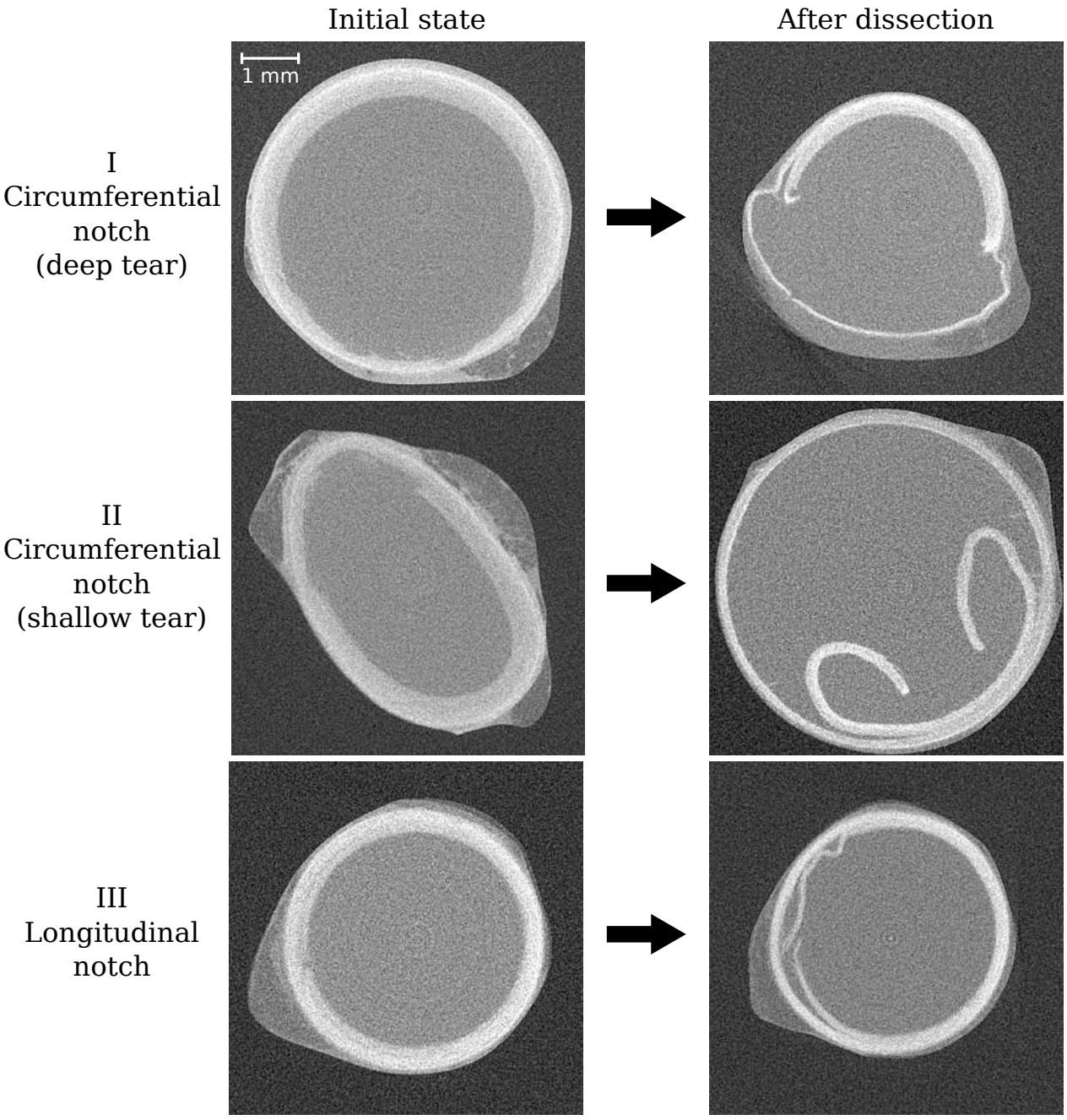

Figure S2: Cross-sections of three specimens at the beginning of the inflation test and after propagation of the dissection. Three different types of initial notches are presented. The initial and final scans were taken at 0 mmHg of pressure. The images show the middle of the sample, where the depth of the notch is the highest. The specimens were named I, II, and III for simplicity. The positions of the notches are bottom in sample I, top-left in sample II, left in sample III. In specimen I, the propagation followed a similar path to the one presented in Figure 3. In sample II the notch propagated on a large part of the circumference but also in the radial-longitudinal plane along the segment. In sample III the notch propagated also in the circumferential direction and in the radial-longitudinal plane.

Influence of intercostal arteries on dissection propagation

During the preparation of the sample, the notch was made between the intercostal arteries in order to avoid any interferences with the dissection. Due to the field of view, it was rarely possible to see the aortic dissection interact with a branch. However, in one of the samples, the dissection was stopped in the circumferential direction by an intercostal artery, leading to the rupture of the aortic wall near the branch ostium, as shown in Figure S3.

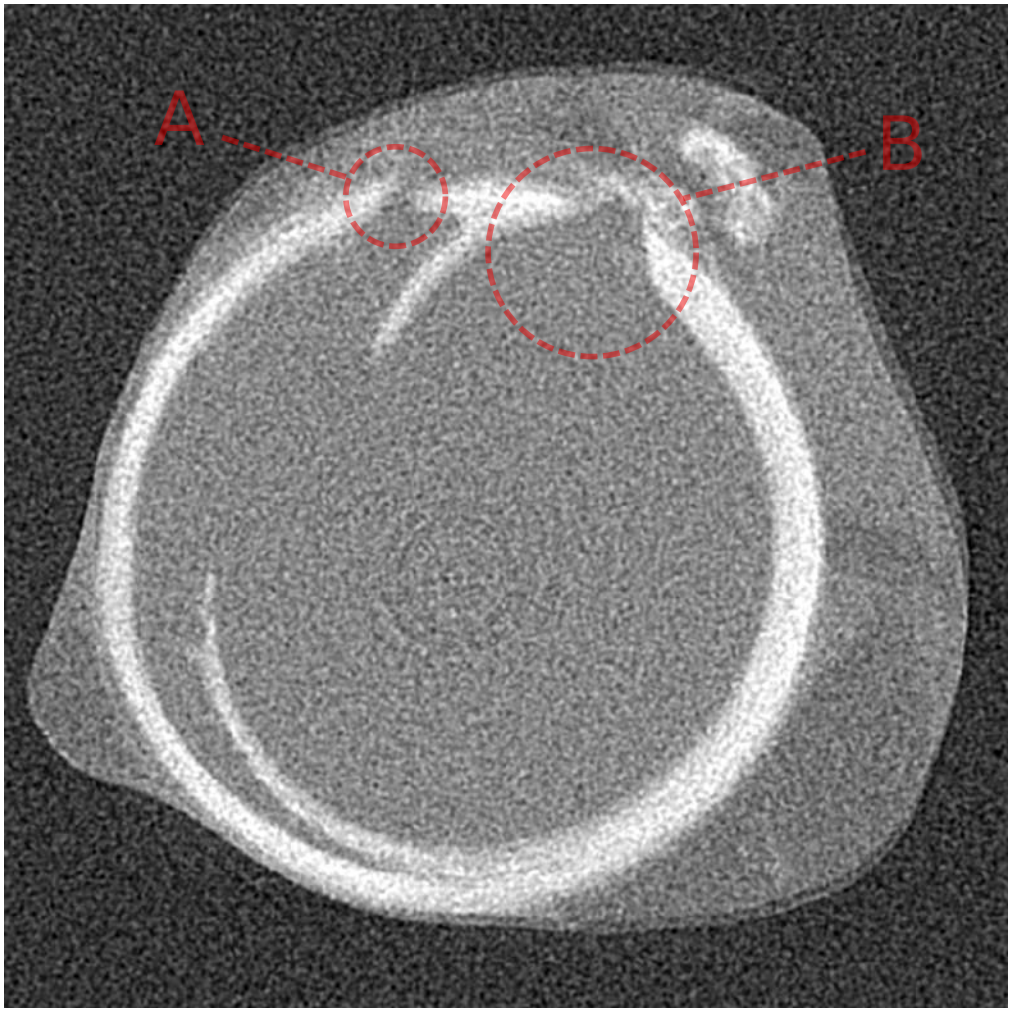

Figure S3: Cross-section of a dissected sample. The circumferential propagation of the notch was stopped by an intercostal branch (B). As a consequence, the wall ruptured near the small branch (A). Conversely, the propagation of the notch in the longitudinal direction was not affected.

Visual artifacts in obtained CT scans

Some visual artifacts are present on the obtained images due to the characteristics of X-ray CT imaging and reconstruction, and should not be interpreted as structural elements of the aortic segments. In particular, a white outline surrounds the outer envelope due to the sudden change in refraction index, and should not be mistaken with the adventitial layer. Besides, white streaks and bands can be seen in heterogeneous regions (e.g. presence of air bubbles) and also surrounding the outer wall. These artifacts are present in Figure 1, 2, 3, 4, 5. 6. Finally, ring artifacts can be seen in Fig. S2 and S3.